

Twofold expansion of the Indo-Pacific warm pool warps the MJO life cycle

<https://doi.org/10.1038/s41586-019-1764-4>

Received: 21 May 2019

Accepted: 17 September 2019

Published online: 27 November 2019

M. K. Roxy^{1,2*}, Panini Dasgupta^{1,3}, Michael J. McPhaden², Tamaki Suematsu⁴, Chidong Zhang² & Daehyun Kim⁵

The Madden–Julian Oscillation (MJO) is the most dominant mode of subseasonal variability in the tropics, characterized by an eastward-moving band of rain clouds. The MJO modulates the El Niño Southern Oscillation¹, tropical cyclones^{2,3} and the monsoons^{4–10}, and contributes to severe weather events over Asia, Australia, Africa, Europe and the Americas. MJO events travel a distance of 12,000–20,000 km across the tropical oceans, covering a region that has been warming during the twentieth and early twenty-first centuries in response to increased anthropogenic emissions of greenhouse gases¹¹, and is projected to warm further. However, the impact of this warming on the MJO life cycle is largely unknown. Here we show that rapid warming over the tropical oceans during 1981–2018 has warped the MJO life cycle, with its residence time decreasing over the Indian Ocean by 3–4 days, and increasing over the Indo-Pacific Maritime Continent by 5–6 days. We find that these changes in the MJO life cycle are associated with a twofold expansion of the Indo-Pacific warm pool, the largest expanse of the warmest ocean temperatures on Earth. The warm pool has been expanding on average by $2.3 \times 10^5 \text{ km}^2$ (the size of Washington State) per year during 1900–2018 and at an accelerated average rate of $4 \times 10^5 \text{ km}^2$ (the size of California) per year during 1981–2018. The changes in the Indo-Pacific warm pool and the MJO are related to increased rainfall over southeast Asia, northern Australia, Southwest Africa and the Amazon, and drying over the west coast of the United States and Ecuador.

Each year, weather variability at subseasonal to seasonal timescales costs the global economy over US\$2 trillion, with US\$700 billion alone in the United States (3.4% of US GDP in 2018)^{12,13}. The MJO contributes to more than 55% of this weather variability over the tropics¹⁴, and modulates the Asian^{4,5}, Australian⁶, African⁷ and American monsoons^{8–10}, tropical cyclogenesis^{2,3} and the El Niño Southern Oscillation (ENSO)¹. The phase and strength of the MJO at a given location can enhance or suppress tropical rainfall variability, modulating or triggering extreme weather events including hurricanes, droughts, flooding, heat waves and cold surges¹⁵. The MJO can also lead to marked effects at mid-latitudes, and is a strong contributor to extreme events in the United States and Europe^{16,17}. The intensity and propagation of the MJO is shown to influence the circulation pattern in the Arctic stratosphere and the polar vortex¹⁸, emphasizing the far-reaching effect of the MJO on the Earth's climate system.

The MJO is an ocean–atmosphere-coupled phenomenon, characterized by eastward moving disturbances of clouds, rainfall, winds and pressure along the Equator. It is the most dominant mode of subseasonal variability in the tropics¹⁹. Using observations and model simulations, previous studies have attempted to understand changes in the MJO in a warming climate²⁰. A link was found between increasing carbon emission and changes in the intensity, frequency and propagation of the MJO over the last few decades of the twentieth century^{20,21}, although

there is considerable uncertainty as to the extent of the changes and the mechanisms involved. A statistical reconstruction of MJO activity over 1905–2008 using tropical surface pressures shows a 13% increase per century in MJO amplitude²². The reconstructed MJO activity agrees with satellite-observed (since 1979) MJO variability on decadal timescales, but the trends disagree after 1997²³, which adds to the considerable uncertainty in these long-term trends. Studies also suggest an increasing trend in MJO frequency after the mid-1970s^{24,25}, which has been linked to long-term warming in the tropical oceans²⁶. Numerical model experiments under idealized global warming scenarios indicate that increasing the surface temperature over the tropical oceans results in an organized MJO activity with a faster eastward propagation^{21,27}, although an understanding based on observations is pending.

Typically, the MJO events are initiated over the Indian Ocean and move eastward over the Maritime Continent to the Pacific (Extended Data Fig. 1). Some of these events weaken or break down over the Maritime Continent or the central Pacific²⁸, but others propagate further to the east Pacific and occasionally continue into the Atlantic²⁹. On average, MJO events travel a zonal distance of 12,000–20,000 km (7,500–12,500 miles) over the generally warm tropical oceans. This entire stretch of the tropical ocean has been warming during the twentieth and early twenty-first centuries in response to greenhouse gas forcing¹¹, and is projected to warm further in the future. The rapid warming across

¹Centre for Climate Change Research, Indian Institute of Tropical Meteorology, Pune, India. ²Pacific Marine Environmental Laboratory, National Oceanic and Atmospheric Administration, Seattle, WA, USA. ³Department of Meteorology and Oceanography, College of Science and Technology, Andhra University, Visakhapatnam, Andhra Pradesh, India. ⁴Atmosphere and Ocean Research Institute, The University of Tokyo, Kashiwa, Chiba, Japan. ⁵Department of Atmospheric Sciences, University of Washington, Seattle, WA, USA. *e-mail: roxy@tropmet.res.in

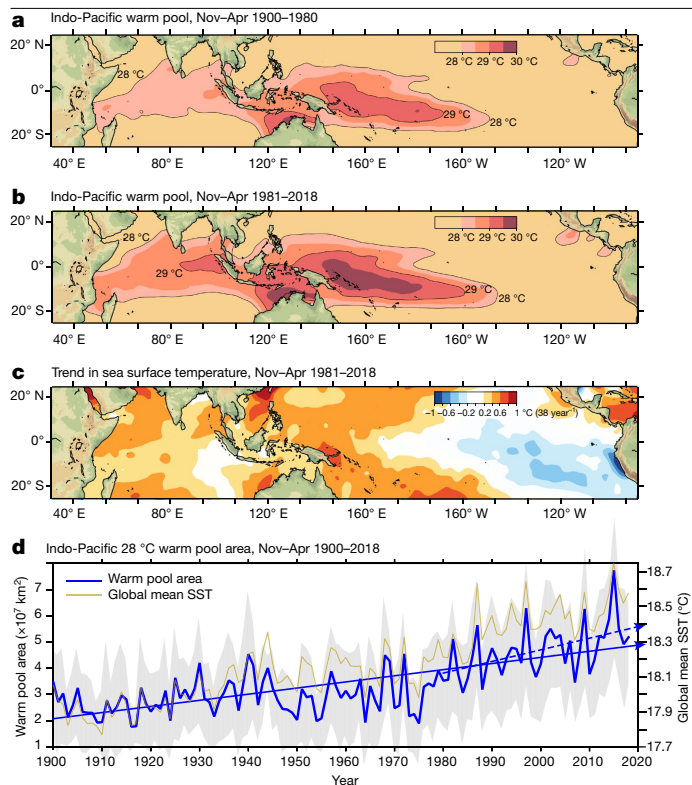


Fig. 1 | A twofold expansion of the warm pool. **a, b**, Indo-Pacific warm pool with its characteristic permanently warm SSTs of greater than 28 °C for the period 1900–1980 (**a**) and 1981–2018 (**b**). The observed warm pool expansion is almost twofold, from an area of 2.2×10^7 km² during 1900–1980, to an area of 4×10^7 km² during 1981–2018. The warm pool area is estimated as the surface area covered by climatological 28 °C isotherm of SST, during November–April, in the tropical Indo-Pacific region within 40° E to 140° W, 25° S to 25° N. **c**, The observed trend in SST (°C per 38 years) during 1981–2018, for November–April. **d**, Time series of the warm pool area during 1900–2018. Theil–Sen trend estimates are overlaid on the time series for the entire period (solid blue line, Sen slope of 2.25×10^5 km² per year) and for 1981–2018 (dashed blue line, Sen slope of 4.14×10^5 km² per year). The positive trend in warm pool area is significant at the 95% confidence level, according to the Mann–Kendall test. The grey shade overlaid on the time series represents \pm two standard deviations of the warm pool area, based on monthly SST values. The yellow line represents global mean SSTs (°C) averaged for November–April. Warm pool SST values and area are based on HadISST dataset. The Generic Mapping Tools (GMT, <https://github.com/GenericMappingTools/gmt>) was used to create the topographic map, with the topography data from ETOPO1 Global Relief Model (<https://www.ngdc.noaa.gov/mgg/global/global.html>).

the tropical basins is not uniform. In the equatorial belt, the largest warming during November–April when the MJO is active is observed over the Indo-Pacific warm pool (Fig. 1). This warm pool is the largest region of permanently warm sea surface temperatures (SSTs >28 °C), covering an area greater than 2.7×10^7 km² (see Methods), over which there is vigorous deep convection. The tropical ocean warming has led to an expansion of this warm pool, particularly in recent decades. Even though there is a preliminary understanding of the general changes in MJO amplitude and frequency in a warming climate, it is not known how the non-uniform ocean warming associated with the expanding warm pool may affect the MJO regionally.

In our study, we find a twofold expansion of the Indo-Pacific warm pool during 1981–2018, in comparison to 1900–1980, with the largest warming occurring over the western Pacific. We show that this warm pool expansion has led to significant changes in the life cycle of MJO events over the Indo-Pacific region. Although the total period of the MJO does not show any detectable trends, its residence time

(MJO phase duration) over the Indian Ocean has been reduced by 3–4 days while over the Maritime Continent its residence time has increased by 5–6 days. Essentially, this means that MJO-related convective activity has grown shorter over the Indian Ocean while the convection over the Maritime Continent is being prolonged.

Observed changes in MJO life cycle

We select the MJO events that exhibit strong coupling between tropical convection and large-scale circulation; prominent active eastward propagation; and an amplitude of the real-time multivariate (RMM) MJO index³⁰ that is greater than one for November–April, 1981–2018 (see Methods). From its normal initiation in the Indian Ocean (RMM phase 1), the MJO propagates into the central Pacific and beyond (phase 8) in about 30–60 days (Extended Data Fig. 2). We compute the average number of days of the selected MJO in each RMM phase to describe the MJO phase duration over the tropical ocean basins. In the RMM index, interannual variations, including those associated with ENSO³⁰, have been removed. This makes it suitable for our investigation focusing on the changes in the MJO related to global warming.

Figure 2 shows the time series of the MJO phase duration and how it has changed over time. The average period of the MJO does not exhibit any detectable trend and broadly remains within the normal timescale of 30–60 days (Extended Data Fig. 2). However, closer inspection (Fig. 2) shows significant changes in individual phases, which essentially are offset while averaging over the entire MJO domain. Over the Indian Ocean (RMM phases 1, 2 and 3), the MJO phase duration decreases by 3–4 days, from an average of 19 days (during 1981–1999) to 15.4 days (during 2000–2018) (Fig. 2a, b). Over the Maritime Continent and the west Pacific (RMM phases 5, 6 and 7), the MJO phase duration increases by 5–6 days, from an average of 17.5 days to 23 days (Fig. 2c, d). The observed trends are statistically significant at the 95% confidence level. The changes are consistent with those documented by previous studies that compared the MJO activity across different RMM phases, using observations and climate model experiments^{31,32}. This means that during recent decades, convective cloud bands associated with the MJO linger over the Indian Ocean for a shorter period, while they persist longer over the Maritime Continent and the west Pacific.

The role of Indo-Pacific warming

SST variations mediate the exchange of heat across the air–sea interface. High SSTs over the tropics are usually accompanied by enhanced convective activity³³. Being an ocean–atmosphere-coupled convective phenomenon, MJO activity is therefore highly dependent on tropical SSTs, with higher MJO activity typically occurring when SSTs are higher²⁶. Previous studies have shown accelerated warming over the Indo-Pacific warm pool and its expansion^{11,34}, which can potentially have an impact on the MJO characteristics. To examine the changes in the warm pool, we estimated the surface area covered by the climatological 28 °C isotherm of SST, during November–April (Fig. 1), in the tropical Indo-Pacific region within 40° E to 140° W, 25° S to 25° N. We show that tropical SST warming has led to an almost twofold expansion of the Indo-Pacific warm pool, from an area of 2.2×10^7 km² during 1900–1980, to an area of 4×10^7 km² during 1981–2018 (Fig. 1a, b, d). The warm pool expansion is non-uniform, with the SST warming more pronounced over the west Pacific in contrast to the Indian Ocean (Fig. 1c). The difference in warm pool expansion trends between the 1900–1980 and 1981–2018 periods is statistically significant at the 95% confidence levels. The shift in warm pool SSTs during the 1977–1980 period co-occur with the shift in global mean SSTs at the same time (Fig. 1d), followed by an accelerated surface warming as a response to anthropogenic emissions³⁵. It is important to note that the shift in SSTs also coincides with the positive phase of the Pacific Decadal Oscillation (PDO). A comparison of the warm pool area using

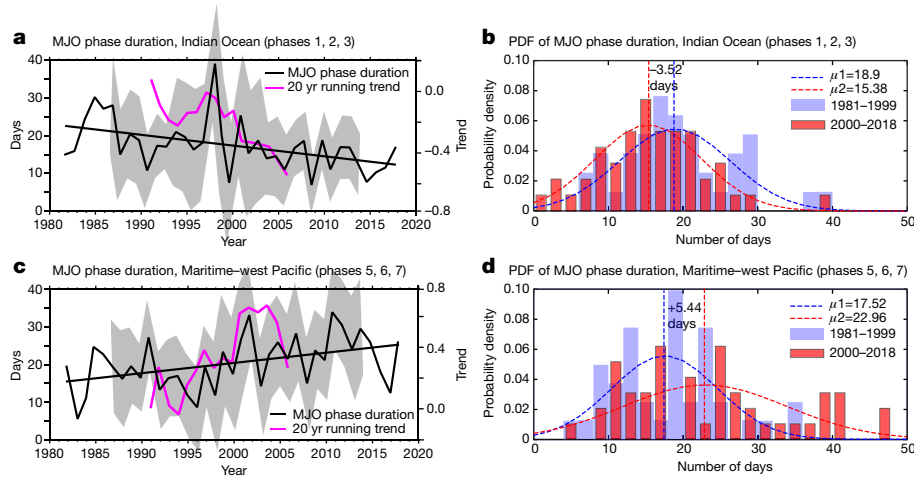


Fig. 2 | Changes in the MJO life cycle. a–d, Time series (black line) and distribution of average yearly phase duration (in days) of MJO events during 1981–2018 over the Indian Ocean (**a, b**; RMM phases 1, 2 and 3) and the Maritime–west Pacific region (**c, d**; RMM phases 5, 6 and 7). Grey shading in **a, c** is \pm two standard deviations of the MJO phase duration over a 10-year moving window. Pink lines overlaid on the time series represent the 20-year running trend of MJO phase duration (in days per year). Mann–Kendall test for the time series indicates that the trends are significant at the 95% confidence level. The

phase duration distribution compares the probability density function (PDF) of MJO phase duration during the earlier period (1981–1999) and later period (2000–2018), where μ_1 and μ_2 represent the mean number of days. $\mu_2 - \mu_1$ indicates the change in MJO phase duration, with a decrease of 3–4 days over the Indian Ocean and increase of 5–6 days over the Maritime–west Pacific region. A Mann–Whitney *U*-test on the difference in the phase duration distributions in **b, d** shows that the difference is statistically robust ($P < 0.05$), implying that the null hypothesis can be rejected.

multiple SST datasets shows that the changes in warm pool area presented here are robust (Extended Data Fig. 3a). A breakpoint analysis confirms that the shifts to higher warm pool values occurred during 1979–1980 (Extended Data Fig. 3b, c).

The changes in the MJO phase duration (phases 5, 6 and 7) appear to be significantly correlated (Fig. 3 and Extended Data Fig. 4) to the changes in SST collocated over the west Pacific warm pool, where the warming trends and the background mean SSTs are the largest. The fact that the correlation is significant even after the trends are removed suggests that the mechanisms working on interannual and longer timescales are similar. Although SST warming is observed in the Indian Ocean also, it is interesting that these SST trends do not show any significant correlation with the MJO phase duration (phases 5, 6 and 7). This might mean that the observed changes in the MJO phase duration are driven by SST changes in the west Pacific. In fact, an investigation of the atmospheric circulation shows enhanced convective activity and a strengthening of low-level westerlies over the west Pacific (120° E to 160° E) associated with trends in the MJO phase duration (Fig. 3b). The enhanced convective activity over the west Pacific is compensated by subsidence over the central and west Indian Ocean (40° E to 70° E). Pohl and Matthews²⁵ hypothesize that on interannual timescales when the west Pacific is warmer than normal, the latent heat release over the moist convective region decreases the effective static stability of the atmosphere and slows down the MJO over the warm pool. The long-term changes in the MJO phase duration and associated ocean–atmospheric interactions discerned here are consistent with the physical mechanisms observed for the MJO phase duration on interannual timescales^{25,36}.

MJO variability and propagation are largely linked to moist static energy in the atmospheric column^{36–38}. For a detailed examination of factors driving the observed trends in the MJO phase duration, we inspected the specific humidity and temperature profiles independently (Fig. 3c). Whereas the MJO trends (phases 5, 6 and 7) exhibit a positive correlation with tropospheric temperatures over the warm pool from 90° E to 170° E, the specific humidity anomalies show a significantly negative correlation over the Indian Ocean and positive correlation over the west Pacific. This indicates that while the warm SST trend in the west Pacific prolongs the local convective activity, it also drives dry air subsidence over the Indian Ocean

(along with the moisture advected away from the basin), shortening the residence time of the MJO over that region. Hence, although the SST over the entire Indo-Pacific is warming, it appears that the MJO response is more sensitive to the west Pacific SST, possibly because the SST trends and background mean values are relatively larger over this region during November–April. Meanwhile, the low-level winds associated with the observed changes in phase duration are westerly over the Indian Ocean (Fig. 3b), converging into the west Pacific. This indicates that the prolonged residence time of the MJO over the Maritime Continent may be supported by moisture supply from both local (west Pacific) and remote (Indian Ocean) sources. Extended Data Figure 5 shows a significant increase in tropospheric moisture (900–400 hPa levels) over the Maritime Continent–west Pacific warm pool region and a reduction in moisture over the Indian Ocean. This is consistent with previous studies³⁹ that suggest that the moisture gradient in the lower troposphere over the Indo-Pacific warm pool assists the eastward propagation of the MJO.

A comparison of the MJO phase duration over the Maritime Continent and west Pacific warm pool area (120° E to 160° E, 25° S to 25° N, highlighted region in Fig. 3, phases 5, 6 and 7) demonstrates a considerable correlation (Pearson correlation, $r = 0.42$; Kendall rank correlation, $\tau = 0.3$) statistically significant at the 95% confidence level (Fig. 3d). The MJO phase duration over the Indian Ocean (phases 1, 2 and 3) also shows a significant negative correlation with the west Pacific ($r = -0.33$), suggesting that the MJO changes over the Indian Ocean are also largely driven by SST warming over the west Pacific. A correlation with the trends removed from both the time series still shows statistical significance at the 90% confidence level, and it can be argued that the results of this analysis strongly hold, even if the large values of the correlation coefficient are due to the existence of a real trend. Furthermore, the mean surface temperatures over the west Pacific also exhibit an interannual variability and long-term change similar to that of the warm pool expansion (Fig. 3d, $r = 0.97$, $\tau = 0.86$). The results presented here establish a clear role of warm pool expansion and increasing SSTs in shortening the residence time of the MJO over the Indian Ocean by 3–4 days and prolonging it over the Maritime Continent by 5–6 days (Extended Data Fig. 6). Such a large change in the MJO phase duration may have direct implications on the global weather and climate, which are tightly linked to these MJO phases.

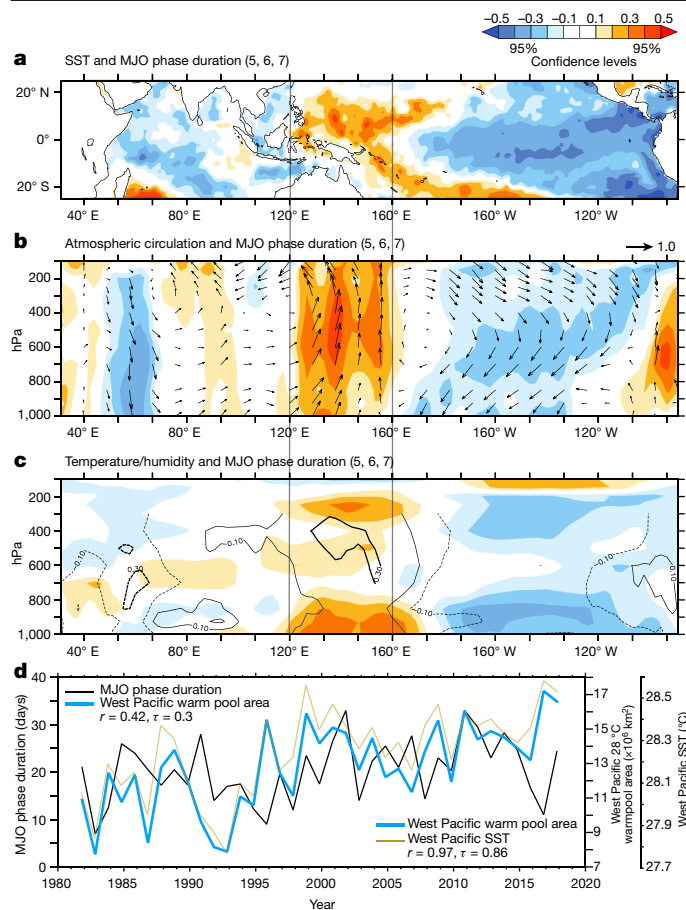


Fig. 3 | Correlation between MJO phase duration and ocean–atmosphere conditions. **a–c**, Correlation between the MJO phase duration (phases 5, 6 and 7) and SST anomalies (**a**), winds and vertical velocity (**b**), and air temperature (colours) and specific humidity (contours) (**c**) at each grid point over the Indo-Pacific basin for November–April, during 1981–2018 ($n = 37$). The correlation analysis is performed after removing the trend and the ENSO variability from the time series. Colour shading denotes correlation coefficients, with the significance at the 95% confidence level noted below the colour scale (above **a**). Vector arrow lengths are proportional to correlation coefficient according to the scale on top of **b**. Thick contours in **c** denote correlation coefficients significant at the 95% confidence level. The region within the solid black lines highlights the west Pacific warm pool region (120° E to 160° E) where the ocean–atmospheric changes related to the MJO phase duration are the largest, and consistent across the various parameters. The longitude–pressure plots are averaged over 10° S to 10° N. **d**, Time series of MJO phase duration (phases 5, 6 and 7) and the surface area (km^2) enclosed by the 28° C isotherm of SST over the west Pacific (120° E to 160° E, 25° S to 25° N), during November–April, 1981–2018. The Kendall rank correlation test (two tailed) for the two variables provided a tau coefficient (τ) of 0.3. The Kendall (τ) and Pearson (r) correlation coefficients shown are significant at the 95% confidence level (significant at the 90% confidence level after removing the trends, $n = 37$). The yellow line overlaid on the time series represents the yearly mean SST over the west Pacific. The Kendall rank correlation test for the west Pacific warm pool area and SST provided a tau coefficient (τ) of 0.86, significant at the 95% confidence level. PyFerret (<http://ferret.pmel.noaa.gov/Ferret/>) was used to generate the map and the plots.

Impacts on global climate

To assess the potential impacts of the observed changes in the MJO phase duration on global climate, we performed a correlation analysis with the rainfall anomalies at each location across the globe, after removing the trends and ENSO-related variability. Figure 4a shows significantly large correlation between observed changes in the MJO phase duration and rainfall variability over tropical and mid-latitude

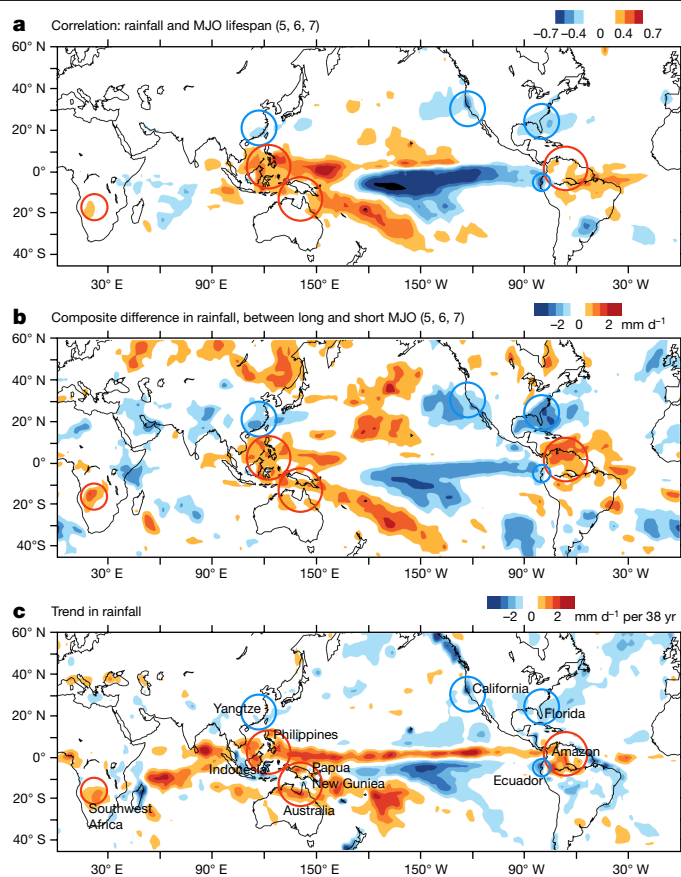


Fig. 4 | Changes in global rainfall in response to the changes in MJO phase duration. **a**, Correlation between the MJO (phases 5, 6 and 7) phase duration and rainfall anomalies for November–April, during 1981–2018. **b**, Composite difference between years when the MJO phase duration (phases 5, 6 and 7) is long and short (above and below one standard deviation). **c**, Observed trend in rainfall (mm day^{-1} per 38 years) during the same period. The correlation and composite analyses are performed after removing the trend and the ENSO variability from the time series. Colour shading denotes correlation coefficients and trends significant at the 95% confidence level. The circled regions indicate large continental areas where the trends in rainfall are consistent with the correlation and composite analyses. Red circles indicate increasing rainfall and blue circles indicate decreasing rainfall associated with the observed changes in the MJO phase duration. Rainfall values are based on the GPCP dataset. The Generic Mapping Tools (GMT, <https://github.com/GenericMappingTools/gmt>) was used to create the map.

regions. The changes in the MJO phase duration over the Indo-Pacific are associated with enhanced rainfall over the Maritime Continent–west Pacific region, the Amazon basin in South America, southwest Africa and northern Australia (colour shades in Fig. 4a indicate correlation coefficients significant at the 95% confidence level). Meanwhile, the changes in MJO phase duration indicate a strong link with reduced rainfall over central and east Pacific, east Africa, the Ganges basin in India, Yangtze basin in China, and the east and west coasts of the United States.

Notably, a trend analysis of rainfall for November–April shows consistent changes over some of these regions (Fig. 4c). An increase in mean rainfall is observed over most of the Maritime Continent, including southeast Asia (Indonesia, Philippines and Papua New Guinea), northern Australia, west Pacific, Amazon basin and southwest Africa. A decline in rainfall is observed over the central Pacific, Ecuador and along the west coast of the United States (California). A slight decrease in rainfall is observed over the Yangtze basin in China and east coast of the United States (Florida), consistent with changes in the MJO phase duration. The observed impacts on rainfall are consistent with the MJO

impacts on interannual timescales reported by previous studies¹⁵, which means that similar processes are operating at interannual and lower frequency timescales (Extended Data Fig. 7). We confirm this with a composite analysis of the MJO events with longer phase duration for phases 5, 6 and 7 (standard deviation greater than one), which shows similar results as for the correlation analysis and the trends (Fig. 4b).

The recent California droughts (2013–2014, during which the MJO was in phases 5, 6 and 7 for 25–28 days), southeast Asia floods (in 2011, during which the MJO was in phases 5, 6 and 7 for 30 days) and east Africa droughts (2011) occurred during those years when the MJO phase duration was longer over the Maritime Continent and the west Pacific (Fig. 2c). Extreme flooding events in Brazil, such as the 2011 Rio de Janeiro floods, have been linked to a strong MJO interacting with the South Atlantic Convergence Zone¹⁰. It cannot be ruled out that the same mean state change (namely warm pool expansion) can affect both the MJO and the regional rainfall changes presented here. In addition, large-scale changes in circulation due to Indo-Pacific warming⁴⁰ and the phase of the PDO could also interact with the MJO to influence the regional rainfall changes observed here. Regardless of their inter-relationship, we can certainly say that the Indo-Pacific warm pool expansion is not only changing the MJO but also these regional precipitation anomalies, either synergistically through the MJO or through independent pathways. Although we have not investigated the dynamics behind these events individually, we cannot overemphasize the need to closely monitor the changes in the Indo-Pacific warm pool for triggering or intensifying severe weather events in the future. Maintaining and enhancing existing ocean observational arrays over the Indian and Pacific basins and extending it to the straits in the southeast Asian maritime region is hence a high priority^{41,42}. Climate model projections suggest further warming of the warm pool region, which may intensify the observed changes in the MJO life cycle in future. However, state-of-the-art climate models fail to accurately simulate the observed distribution of SST changes over the Indo-Pacific even in the present climate, and hence may need further improvement (for example, via the subseasonal to seasonal prediction project^{42,43}) in order to meet the challenges presented by a warming world.

Online content

Any methods, additional references, Nature Research reporting summaries, source data, extended data, supplementary information, acknowledgements, peer review information; details of author contributions and competing interests; and statements of data and code availability are available at <https://doi.org/10.1038/s41586-019-1764-4>.

- McPhaden, M. J. Genesis and evolution of the 1997–98 El Niño. *Science* **283**, 950–954 (1999).
- Maloney, E. D. & Hartmann, D. L. Modulation of eastern North Pacific hurricanes by the Madden–Julian oscillation. *J. Clim.* **13**, 1451–1460 (2000).
- Klotzbach, P. J. & Oliver, E. C. Modulation of Atlantic basin tropical cyclone activity by the Madden–Julian oscillation (MJO) from 1905 to 2011. *J. Clim.* **28**, 204–217 (2015).
- Joseph, S., Sahai, A. & Goswami, B. Eastward propagating MJO during boreal summer and Indian monsoon droughts. *Clim. Dyn.* **32**, 1139–1153 (2009).
- Jia, X., Chen, L., Ren, F. & Li, C. Impacts of the MJO on winter rainfall and circulation in China. *Adv. Atmos. Sci.* **28**, 521–533 (2011).
- Wheeler, M. C., Hendon, H. H., Cleland, S., Meinke, H. & Donald, A. Impacts of the Madden–Julian oscillation on Australian rainfall and circulation. *J. Clim.* **22**, 1482–1498 (2009).
- Pohl, B. & Camberlin, P. Influence of the Madden–Julian oscillation on East African rainfall. I: intraseasonal variability and regional dependency. *Q. J. R. Meteorol. Soc.* **132**, 2521–2539 (2006).
- Lorenz, D. J. & Hartmann, D. L. The effect of the MJO on the North American monsoon. *J. Clim.* **19**, 333–343 (2006).
- Grimm, A. M. Madden–Julian Oscillation impacts on South American summer monsoon season: precipitation anomalies, extreme events, teleconnections, and role in the MJO cycle. *Clim. Dyn.* **53**, 1–26 (2019).

- Carvalho, L. M. V., Jones, C. & Liebmann, B. The South Atlantic convergence zone: intensity, form, persistence, and relationships with intraseasonal to interannual activity and extreme rainfall. *J. Clim.* **17**, 88–108 (2004).
- Weller, E. et al. Human-caused Indo-Pacific warm pool expansion. *Sci. Adv.* **2**, e1501719 (2016).
- Lazo, J. K., Lawson, M., Larsen, P. H. & Waldman, D. M. US economic sensitivity to weather variability. *Bull. Am. Meteorol. Soc.* **92**, 709–720 (2011).
- Bertrand, J.-L. & Brusset, X. Managing the financial consequences of weather variability. *J. Asset Manag.* **19**, 301–315 (2018).
- Kessler, W. S. EOF representations of the Madden–Julian oscillation and its connection with ENSO. *J. Clim.* **14**, 3055–3061 (2001).
- Zhang, C. Madden–Julian oscillation: bridging weather and climate. *Bull. Am. Meteorol. Soc.* **94**, 1849–1870 (2013).
- Cassou, C. Intraseasonal interaction between the Madden–Julian Oscillation and the North Atlantic Oscillation. *Nature* **455**, 523–527 (2008).
- Stan, C. et al. Review of tropical-extratropical teleconnections on intraseasonal time scales. *Rev. Geophys.* **55**, 902–937 (2017).
- Garfinkel, C. I., Feldstein, S. B., Waugh, D. W., Yoo, C. & Lee, S. Observed connection between stratospheric sudden warmings and the Madden–Julian Oscillation. *Geophys. Res. Lett.* **39**, L18807 (2012).
- Madden, R. A. & Julian, P. R. Observations of the 40–50-day tropical oscillation—a review. *Mon. Weath. Rev.* **122**, 814–837 (1994).
- Maloney, E. D., Adames, Á. F. & Bui, H. X. Madden–Julian oscillation changes under anthropogenic warming. *Nat. Clim. Change* **9**, 26–33 (2019).
- Adames, Á. F., Kim, D., Sobel, A. H., Del Genio, A. & Wu, J. Changes in the structure and propagation of the MJO with increasing CO₂. *J. Adv. Model. Earth Syst.* **9**, 1251–1268 (2017).
- Oliver, E. C. & Thompson, K. R. A reconstruction of Madden–Julian Oscillation variability from 1905 to 2008. *J. Clim.* **25**, 1996–2019 (2012).
- Oliver, E. C. Blind use of reanalysis data: apparent trends in Madden–Julian Oscillation activity driven by observational changes. *Int. J. Climatol.* **36**, 3458–3468 (2016).
- Jones, C. & Carvalho, L. M. V. Changes in the activity of the Madden–Julian Oscillation during 1958–2004. *J. Clim.* **19**, 6353–6370 (2006).
- Pohl, B. & Matthews, A. J. Observed changes in the lifetime and amplitude of the Madden–Julian oscillation associated with interannual ENSO sea surface temperature anomalies. *J. Clim.* **20**, 2659–2674 (2007).
- Slingo, J. M., Rowell, D. P., Sperber, K. R. & Nortley, E. On the predictability of the interannual behaviour of the Madden–Julian Oscillation and its relationship with El Niño. *Q. J. R. Meteorol. Soc.* **125**, 583–609 (1999).
- Arnold, N. P., Kuang, Z. & Tziperman, E. Enhanced MJO-like variability at high SST. *J. Clim.* **26**, 988–1001 (2013).
- Zhang, C. & Ling, J. Barrier effect of the Indo-Pacific Maritime Continent on the MJO: perspectives from tracking MJO precipitation. *J. Clim.* **30**, 3439–3459 (2017).
- Foltz, G. R. & McPhaden, M. J. The 30–70 day oscillations in the tropical Atlantic. *Geophys. Res. Lett.* **31**, L15205 (2004).
- Wheeler, M. C. & Hendon, H. H. An all-season real-time multivariate MJO index: development of an index for monitoring and prediction. *Mon. Weath. Rev.* **132**, 1917–1932 (2004).
- Yoo, C., Feldstein, S. & Lee, S. The impact of the Madden–Julian Oscillation trend on the Arctic amplification of surface air temperature during the 1979–2008 boreal winter. *Geophys. Res. Lett.* **38**, L24804 (2011).
- Song, E. J. & Seo, K. H. Past-and present-day Madden–Julian Oscillation in CNRM-CM5. *Geophys. Res. Lett.* **43**, 4042–4048 (2016).
- Roxy, M. Sensitivity of precipitation to sea surface temperature over the tropical summer monsoon region—and its quantification. *Clim. Dyn.* **43**, 1159–1169 (2014).
- Cravatte, S., Delcroix, T., Zhang, D., McPhaden, M. & Leloup, J. Observed freshening and warming of the western Pacific warm pool. *Clim. Dyn.* **33**, 565–589 (2009).
- Dong, L. & McPhaden, M. J. The role of external forcing and internal variability in regulating global mean surface temperatures on decadal timescales. *Environ. Res. Lett.* **12**, 034011 (2017).
- Suematsu, T. & Miura, H. Zonal SST difference as a potential environmental factor supporting the longevity of the Madden–Julian Oscillation. *J. Clim.* **31**, 7549–7564 (2018).
- Sobel, A., Wang, S. & Kim, D. Moist static energy budget of the MJO during DYNAMO. *J. Atmos. Sci.* **71**, 4276–4291 (2014).
- Kim, D., Kug, J.-S. & Sobel, A. H. Propagating versus nonpropagating Madden–Julian Oscillation events. *J. Clim.* **27**, 111–125 (2014).
- Gonzalez, A. O. & Jiang, X. Winter mean lower tropospheric moisture over the Maritime Continent as a climate model diagnostic metric for the propagation of the Madden–Julian oscillation. *Geophys. Res. Lett.* **44**, 2588–2596 (2017).
- Tokina, H., Xie, S.-P., Deser, C., Kosaka, Y. & Okumura, Y. M. Slowdown of the Walker circulation driven by tropical Indo-Pacific warming. *Nature* **491**, 439–443 (2012).
- Hermes, J. C. et al. A sustained ocean observing system in the Indian Ocean for climate related scientific knowledge and societal needs. *Front. Mar. Sci.* **6**, 355 (2019).
- Subramanian, A. et al. Ocean observations to improve our understanding, modeling, and forecasting of subseasonal-to-seasonal variability. *Front. Mar. Sci.* **6**, 427 (2019).
- Vitar, F. & Robertson, A. W. The sub-seasonal to seasonal prediction project (S2S) and the prediction of extreme events. *npj Clim. Atmos. Sci.* **1**, 3 (2018).

Publisher's note Springer Nature remains neutral with regard to jurisdictional claims in published maps and institutional affiliations.

© The Author(s), under exclusive licence to Springer Nature Limited 2019

Methods

MJO data and identification of events

The real-time multivariate MJO (RMM) index of Wheeler and Hendon³⁰, provided by the Australian Bureau of Meteorology, is used as a preliminary reference for identifying MJO events during 1981–2018. The RMM index³⁰ relies on an Empirical Orthogonal Function analysis, which combines equatorially averaged (15° S to 15° N) lower (850 hPa) and upper (200 hPa) tropospheric zonal winds with outgoing longwave radiation (OLR, proxy indicator for convective activity). Although the RMM index efficiently captures the dominant role of zonal winds during mature phases of strong MJO events, it can be inconsistent in representing the convective conditions associated with it^{44–46}. As a result of this absence of interplay between circulation and convection, capturing the MJO events with its convective implications has been a conundrum, as the index occasionally captures non-existent events, while some events appear to occur early or late, or are even missing^{28,44–47}.

Hence, we identified MJO events by following a set of steps that consider the RMM index but clearly capture the MJO characteristics of eastward propagation and convective activity. We focus on the boreal autumn–winter–spring seasons (November–April) during which the MJO exhibits a prominent eastward propagation, and is sensitive to SST variations in the Indian and Pacific oceans⁴⁸. In order to factor in the convective activity, we used the daily OLR from the National Oceanic and Atmospheric Administration (NOAA) at 2.5° × 2.5° horizontal resolution, which has been conventionally used for detecting the MJO-related convective activity. We also verified the detected events using the high-resolution (1° × 1°) daily OLR Climate Data Record⁴⁹, which is better suited for identifying the tropical variability at sub-seasonal timescales⁵⁰. The MJO phase duration is strongly linked to the strength of MJO convection and its coupling with the largescale circulation⁵¹. Hence, the current method makes sure to capture the MJO events that exhibit strong coupling between tropical convection and largescale circulation.

The OLR on subseasonal timescales also represents other types of equatorial propagating modes of convection, such as the westward-moving equatorial Rossby waves, eastward-moving Kelvin waves and mixed Rossby–gravity waves. The MJO component is therefore filtered from the OLR data by including eastward zonal wavenumbers 1–5 and a period of 30–96 days, while the Kelvin wave component is separated by identifying eastward wavenumbers 1–14 and a period of 2–30 days, and equatorial Rossby waves by their westward zonal wavenumbers 1–10 and periods of 10–50 days^{52,53}. We select eastward propagating convective MJO events in the filtered OLR anomalies, which are initiated in the Indian Ocean (phases 1, 2 or 3)²⁸, proceed to the Pacific (phases 6, 7 or 8) and propagate through at least six of the RMM phases with an average RMM amplitude greater than one (-1.5 standard deviation). We consider the initiation date as when the RMM index indicates MJO entry into the Indian Ocean from the west and starts to propagate eastward. We find 88 such MJO events over the 38 years, during November–April. The selected events are comparable to the MJO events detected by the tracking method used by Suematsu and Miura³⁶, which is based solely on the RMM index at a threshold amplitude of 0.8, but with a relatively wide window for the band-pass filter (20–120 days).

Note that for computational purposes, the data for November–April are considered together as belonging to the initial year (for example, MJO activity during November 1981–April 1982 is considered together as representing the year 1981). Hence, although we have 38 years of data, we consider it as 37 MJO seasons.

Warm pool SST and climate data analysis

HadISST1 SST data for the period 1900–2018, obtained from the Met Office Hadley Centre, is used to estimate the changes in the Indo-Pacific warm pool and its role on the MJO phase duration. The warm pool area is estimated as the surface area covered by the climatological 28 °C

isotherm of SST, during November–April (Fig. 1), in the tropical Indo-Pacific region within 40° E to 140° W, 25° S to 25° N. To examine the state and response of atmospheric circulation to the changing SSTs and MJO, we used air temperature, winds and specific humidity values for the tropospheric column from NCEP reanalysis for the period 1981–2018 at a 2.5° × 2.5° grid resolution. The global changes in rainfall are estimated using the NOAA GPCP precipitation dataset, which combines observations and satellite precipitation data on a 2.5° × 2.5° global grid.

A breakpoint analysis⁵⁴ is conducted to identify significant shifts in the mean of the Indo-Pacific warm pool time series (Extended Data Fig. 3b). The analysis uses a Bai–Perron test⁵⁵ to determine the optimal number of breaks using Bayesian information criterion⁵⁶ and the residual sum of squares, given the minimum segment size of the time series (30 year segments used here). The location of these breakpoints can be attributed to the timing of nonlinear changes in the observed warm pool area over time. The analysis was performed using the ‘strucchange’ package in the R Statistical Software⁵⁴.

The life cycle of the MJO and the tropical ocean–atmosphere conditions are also dependent on the state of the ENSO. We use a frequency bandpass filter (2–6 years) to remove the interannual frequency band associated with ENSO-related variations, although removing all of the ENSO related variability is difficult as it can influence variability at both higher and lower frequency. The correlation analysis and trends in Figs. 3 and 4 are estimated using these filtered anomalies. The least-square linear regression and Theil–Sen slope methods are used to estimate the observed trends. The Theil–Sen approach is considered more robust than the least-squares method due to its relative insensitivity to extreme values and better performance even for normally distributed data⁵⁷.

The statistical significance of the trends, correlations and the difference of slopes⁵⁸ (Extended Data Fig. 3c) is examined using standard two-tailed Student’s *t*-tests. The significance of the trends in the time series plots are further assessed with a Mann–Kendall test with block bootstrap to validate the significance when a time series shows autocorrelation⁵⁹. Statistical significance exceeding the 95% confidence level is selected a priori as the level at which the null hypothesis can be rejected. The correlation analysis is also tested using Kendall rank correlation that is non-parametric and therefore makes no assumptions about the distribution and at the same time determine the direction and significance of the relation between the two variables⁵⁹. The correlated variables are said to be concordant if their ranks vary together (+1) and discordant if they vary differently (-1). In order to compare the differences in the distribution of the MJO phase durations in Fig. 2, we have used the Mann–Whitney *U*-test⁶⁰ to test the null hypothesis that there is no difference between two means (Extended Data Fig. 8). The Mann–Whitney *U*-test is a non-parametric test useful for relatively short time series, and also takes into account the fact that MJO variability is not normally distributed about the mean state.

Data availability

The MJO RMM index used in the study for the period 1981–2018 is available from the Australian Bureau of Meteorology (<http://www.bom.gov.au/climate/mjo/>). The monthly values of air temperature, specific humidity and winds, and the daily OLR and GPCP monthly precipitation can be obtained from the NOAA website (<https://www.esrl.noaa.gov/psd/data/gridded/>). HadISST data are available for download at the Met Office Hadley Centre website (<https://www.metoffice.gov.uk/hadobs/hadisst/>). The high-resolution daily OLR data can be acquired from the University of Maryland OLR CDR portal (<http://olr.umd.edu/>).

Code availability

The MJO events identified in this study, and the code for estimating the individual MJO phase duration and the Indo-Pacific warm pool area,

are available at <https://github.com/RoxyKoll/warmpool-mjo>. The code for filtering the MJO component from the OLR data is available from C. Schreck at GitLab (https://k3.cicsnc.org/carl/carl-ncl-tools/blob/master/filter/filter_waves.ncl).

44. Straub, K. H. MJO initiation in the real-time multivariate MJO index. *J. Clim.* **26**, 1130–1151 (2013).
45. Liu, P. et al. A revised real-time multivariate MJO index. *Mon. Weath. Rev.* **144**, 627–642 (2016).
46. Wolding, B. O. & Maloney, E. D. Objective diagnostics and the Madden–Julian oscillation. Part II: application to moist static energy and moisture budgets. *J. Clim.* **28**, 7786–7808 (2015).
47. Ventrice, M. J. et al. A modified multivariate Madden–Julian oscillation index using velocity potential. *Mon. Weath. Rev.* **141**, 4197–4210 (2013).
48. Hendon, H. H., Wheeler, M. C. & Zhang, C. Seasonal dependence of the MJO–ENSO relationship. *J. Clim.* **20**, 531–543 (2007).
49. Schreck, C., Lee, H.-T. & Knapp, K. HIRS outgoing longwave radiation—daily climate data record: application toward identifying tropical subseasonal variability. *Remote Sens.* **10**, 1325 (2018).
50. Kikuchi, K., Wang, B. & Kajikawa, Y. Bimodal representation of the tropical intraseasonal oscillation. *Clim. Dyn.* **38**, 1989–2000 (2012).
51. Seo, K.-H. & Kumar, A. The onset and life span of the Madden–Julian oscillation. *Theor. Appl. Climatol.* **94**, 13–24 (2008).
52. Wheeler, M. & Kiladis, G. N. Convectively coupled equatorial waves: analysis of clouds and temperature in the wavenumber–frequency domain. *J. Atmos. Sci.* **56**, 374–399 (1999).
53. Roundy, P. E., Schreck, C. J. III & Janiga, M. A. Contributions of convectively coupled equatorial Rossby waves and Kelvin waves to the real-time multivariate MJO indices. *Mon. Weath. Rev.* **137**, 469–478 (2009).
54. Zeileis, A., Kleiber, C., Krämer, W. & Hornik, K. Testing and dating of structural changes in practice. *Comput. Stat. Data Anal.* **44**, 109–123 (2003).
55. Bai, J. & Perron, P. Computation and analysis of multiple structural change models. *J. Appl. Econ.* **18**, 1–22 (2003).
56. Schwarz, G. Estimating the dimension of a model. *Ann. Stat.* **6**, 461–464 (1978).
57. Hirsch, R. M., Slack, J. R. & Smith, R. A. Techniques of trend analysis for monthly water quality data. *Wat. Resour. Res.* **18**, 107–121 (1982).
58. Cohen, P., West, S. G. & Aiken, L. S. *Applied Multiple Regression/Correlation Analysis for the Behavioral Sciences* (Psychology Press, 2014).
59. Kendall, M. G. *Rank Correlation Methods* 2 edn (C. Griffin, 1948).
60. Mann, H. B. & Whitney, D. R. On a test of whether one of two random variables is stochastically larger than the other. *Ann. Math. Stat.* **18**, 50–60 (1947).

Acknowledgements M.K.R. acknowledges NOAA/PMEL for the National Research Council Senior Research Associateship Award by the US National Academy of Sciences (PMEL contribution no. 4975). P.D. was supported by the ITM Research Fellowship. D.K. was supported by the DOE RGMA program (DE-SC0016223), the NOAA CVP program (NA18OAR4310300), and the KMA R&D program (KMI2018-03110). We thank N. Bond and R. Murtugudde for their comments on an early draft of this manuscript.

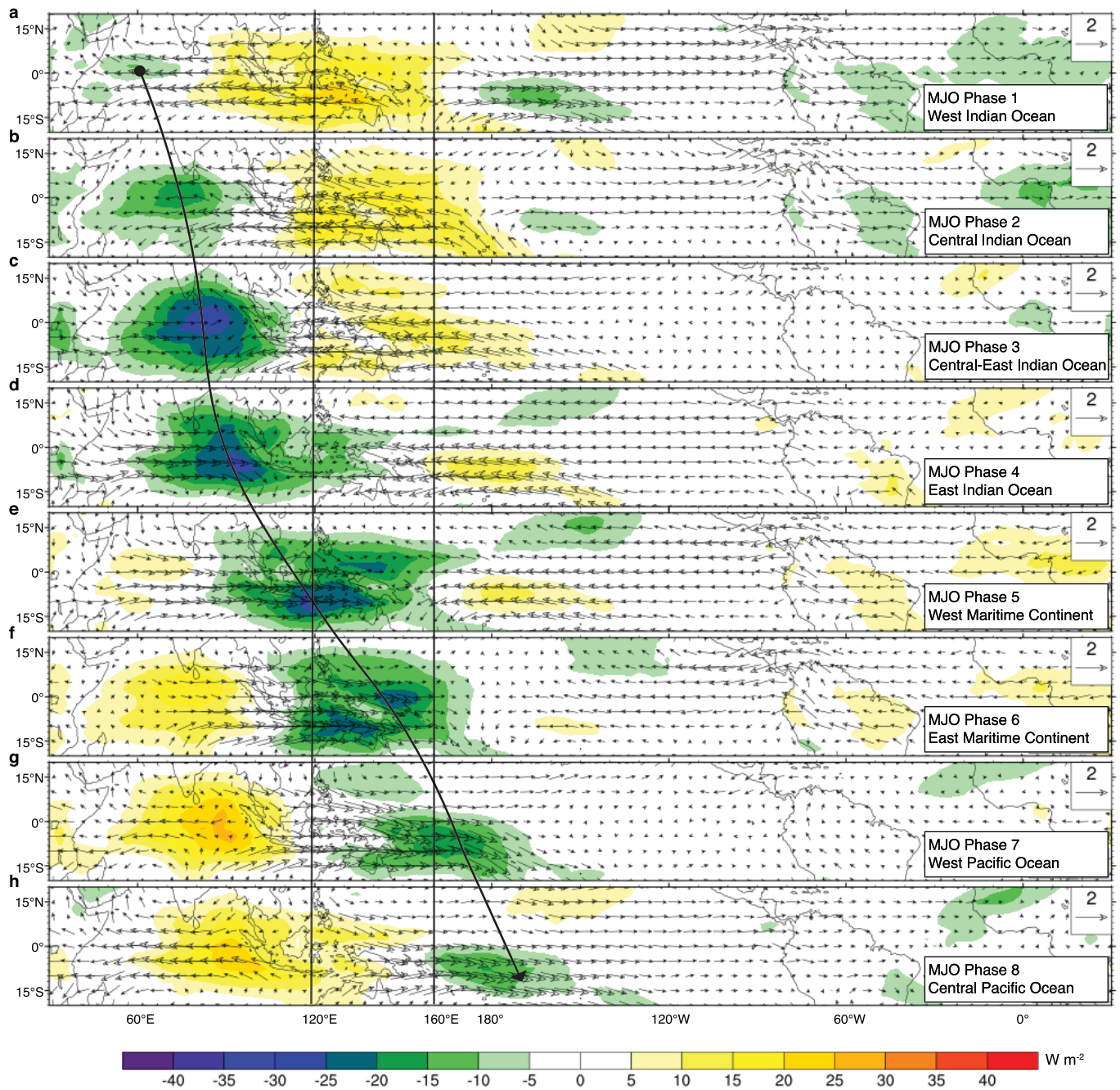
Author contributions M.K.R. conceived the study, performed the analysis and prepared the manuscript. P.D. performed the MJO detection and initial analysis. T.S. provided additional MJO tracking algorithm for verification. All co-authors contributed to the interpretation of the results and drafting of the manuscript for publication.

Competing interests The authors declare no competing interests.

Additional information

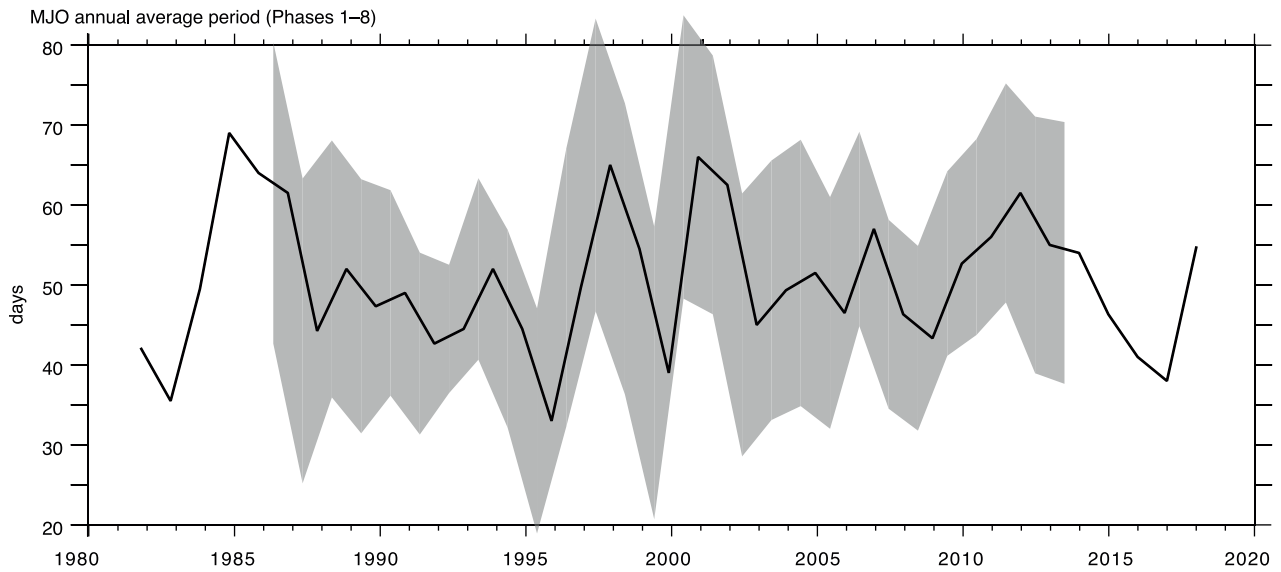
Correspondence and requests for materials should be addressed to M.K.R.

Reprints and permissions information is available at <http://www.nature.com/reprints>.

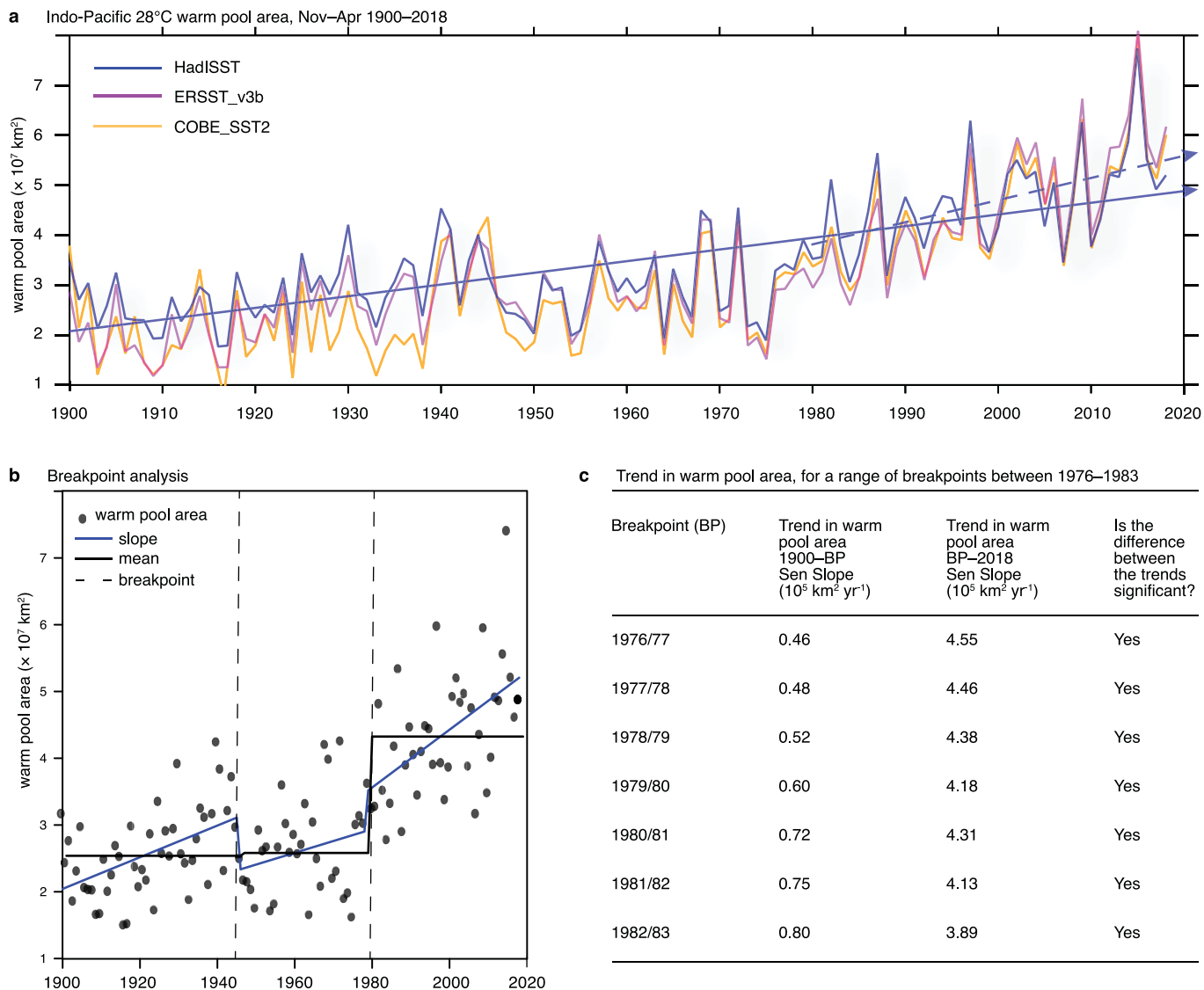


Extended Data Fig. 1 | Typical life cycle of the MJO. Composite anomalies of 30–100 day OLR (W m^{-2}) during November–April, for the period 1981–2018, showing the RMM phases 1–8. Typically, the MJO events are initiated over the Indian Ocean and move eastward over the Maritime Continent to the Pacific (a–h). The region within the solid black lines highlight the west Pacific warm

pool region (120°E to 160°E) where ocean–atmospheric changes related to the MJO lifespan are the largest. OLR values are based on the NOAA interpolated OLR dataset. The NCAR Command Language (NCL, <http://ncl.ucar.edu>) is used to plot the MJO life cycle on the map.

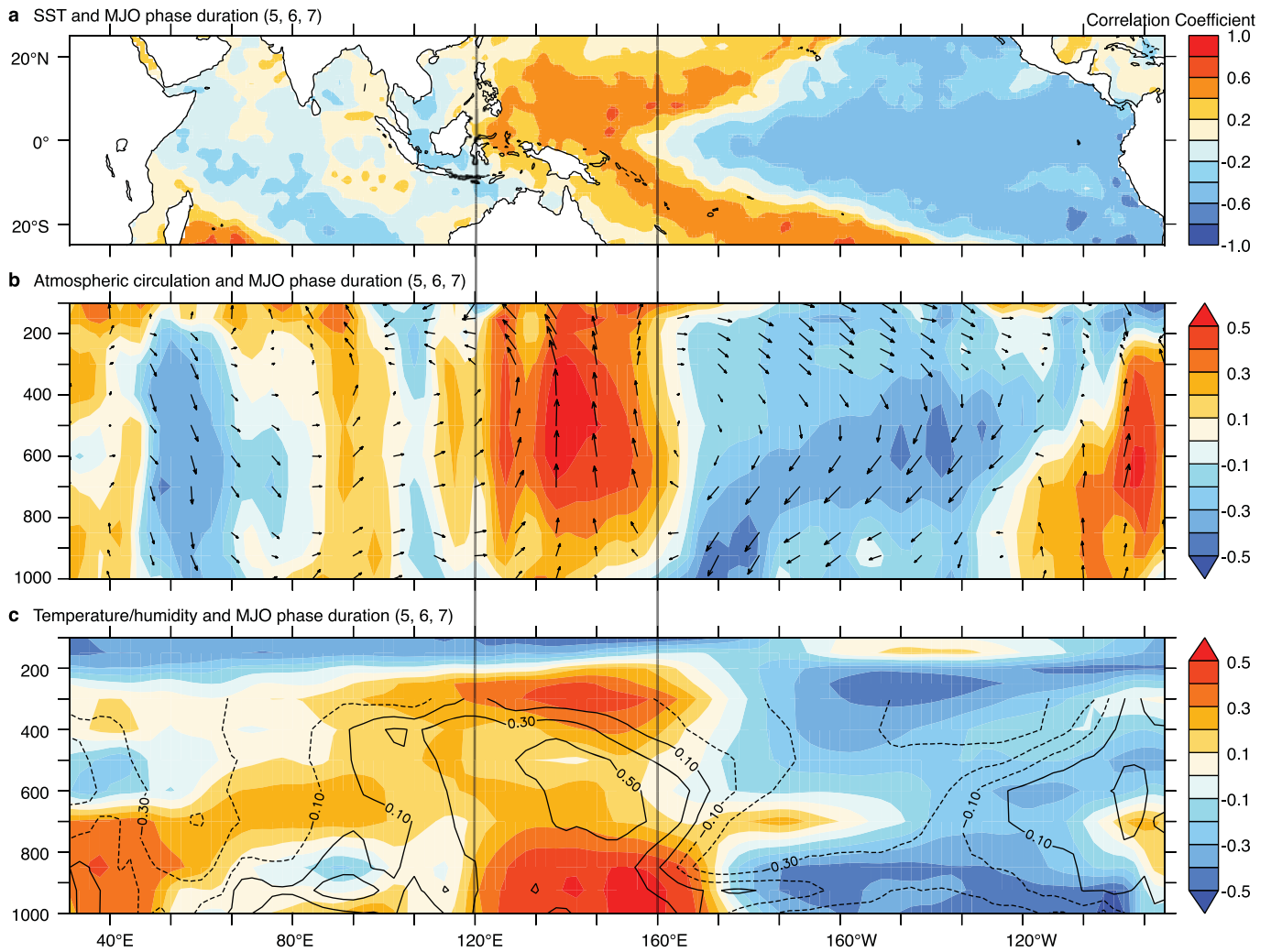


Extended Data Fig. 2 | Annual average period of MJO events. Time series of yearly average period of MJO events during November–April, 1981–2016 (phases 1–8). The grey shade overlaid on the time series represents \pm two standard deviations of the MJO phase duration over a 10-year moving window.



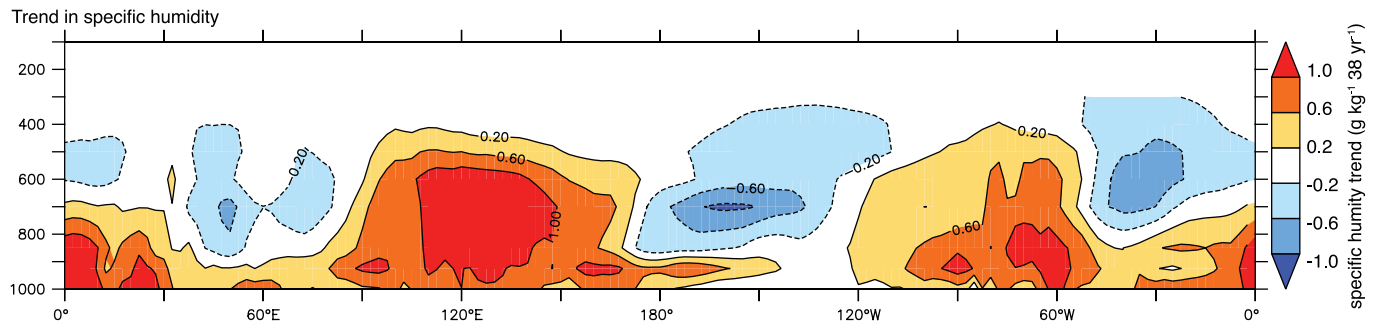
Extended Data Fig. 3 | Warm pool area in multiple datasets and breakpoint analysis. **a**, Time series of the warm pool area during November–April, 1900–2018, based on HadISST, ERSST_v3b and COBE_SST2 datasets. Their Sen trend estimates computed based on HadISST (as in Fig. 1) are overlaid on the time series for the entire period (solid blue line) and for 1981–2018 (dashed blue line). **b**, Breakpoint analysis identifying the significant shifts in the mean of the Indo-Pacific warm pool time series, using HadISST. The breakpoint analysis shows two shifts in the time series, the first during 1945–1946 and the second during 1979–1980. Although the rate of change in warm pool area during 1900–1945

and 1946–1979 are different, the average warm pool area remains almost the same during both the periods. The breakpoint analysis confirms that the shifts to higher warm pool values occurred in the annual series during 1979–1980. **c**, Table showing the trend in warm pool area using a range of breakpoints, from 1976–1977 to 1982–1983. The rate of warming does not change substantially with different breakpoints. At the same time, the difference between the trends is significant for all breakpoints considered. The significance of the difference between the slopes is estimated based on a *t*-test⁵⁸.



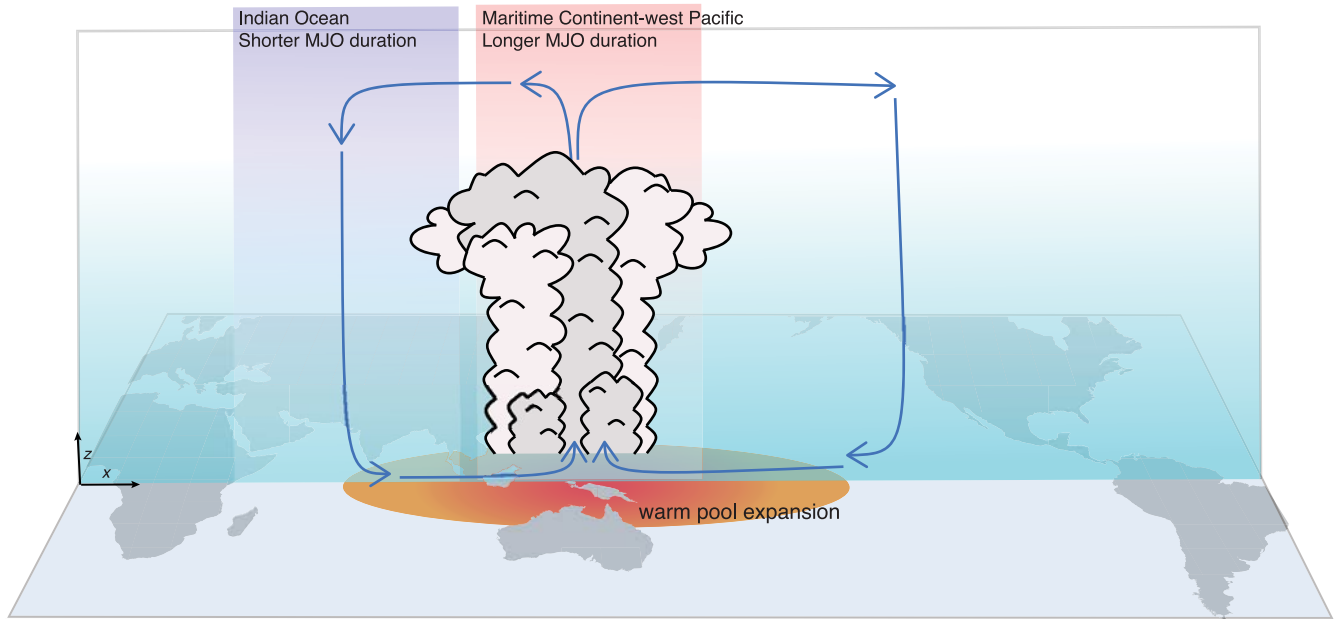
Extended Data Fig. 4 | Correlation between MJO phase duration and ocean-atmosphere conditions, without removing the trends. a–c, Correlation between yearly average of MJO phase distribution (phases 5, 6 and 7) with (a) SST anomalies, (b) winds and vertical velocity and (c) air temperature (colours) and specific humidity (contours) over the Indo-Pacific basin for November–

April, during 1981–2018 ($n = 37$). The correlation analyses are performed after removing the ENSO variability from the time series, but without removing the trends. PyFerret (<http://ferret.pmel.noaa.gov/Ferret/>) is used to generate the map and the plots.

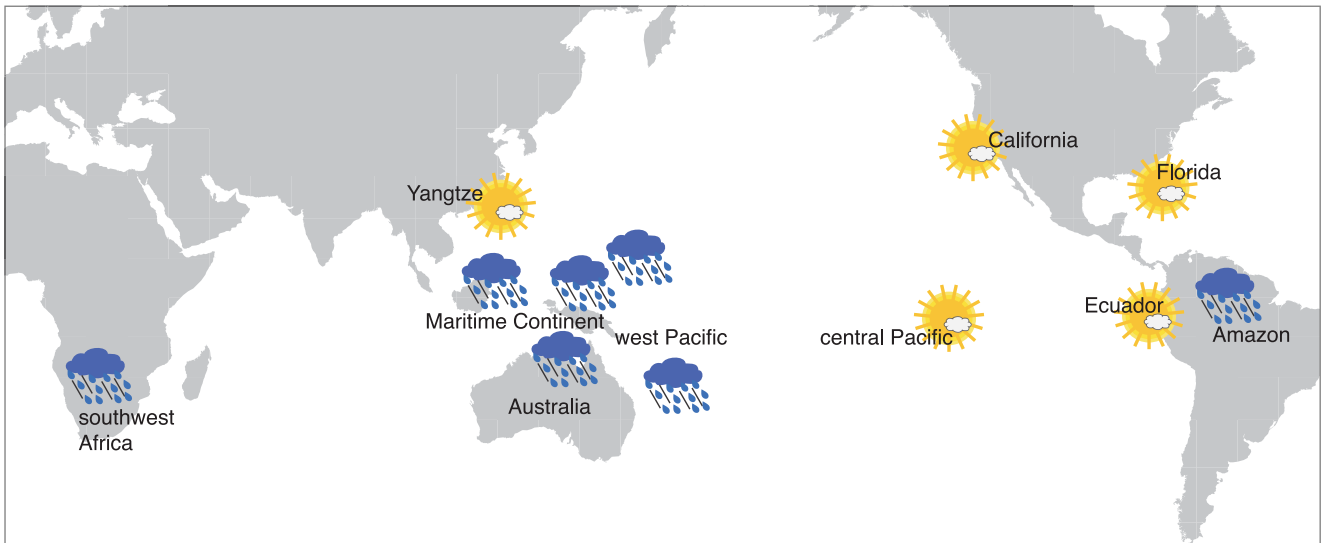


Extended Data Fig. 5 | Trend in specific humidity anomalies. Trend in specific humidity anomalies (g kg^{-1} per 38 years) for November–April, during 1981–2018. The trends indicate an increase (red colours) in tropospheric moisture over the warm pool region and a reduction (blue colours) in tropospheric moisture over the Indian Ocean (900–400 hPa levels).

a Indo-Pacific warm pool expansion warps MJO lifecycle



b Impacts on global climate

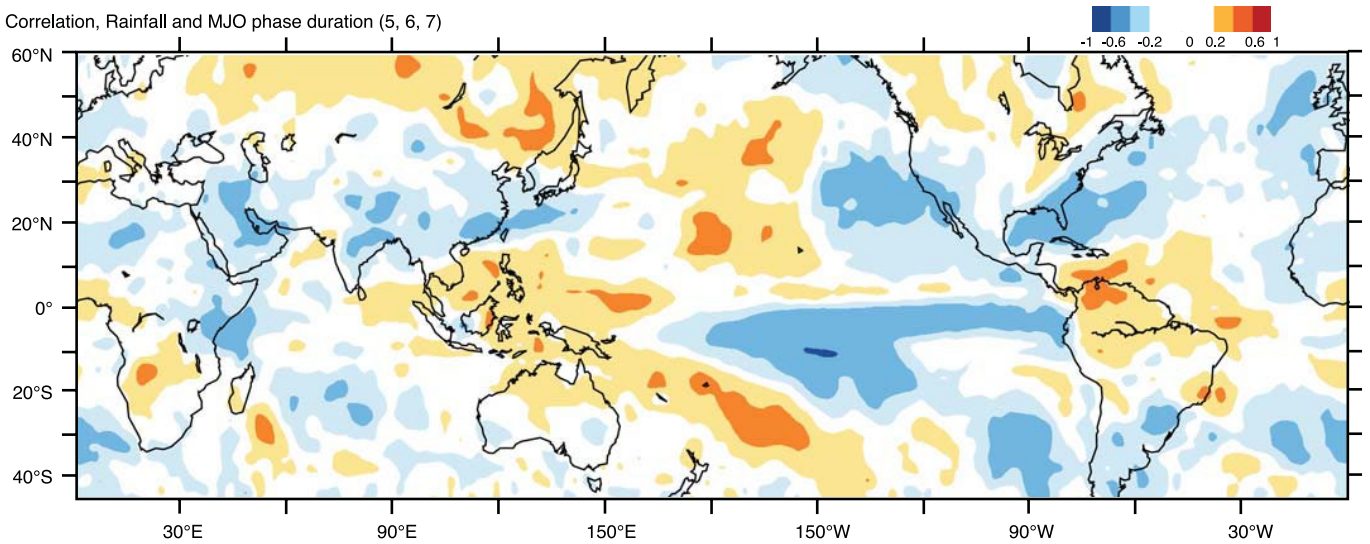


Extended Data Fig. 6 | Schematics showing the changes in MJO life cycle and impact on the global climate. a, As the Indo-Pacific warm pool expands with increasing SSTs, moist winds converge over the Maritime Continent–west Pacific, prolonging the MJO phase duration over this region by 5–6 days and shortening the MJO duration over the Indian Ocean by 3–4 days. **b**, As a response to the changes in the MJO phase duration, an increase in mean rainfall

is observed over most of the Maritime Continent including southeast Asia, and over northern Australia, west Pacific, Amazon basin and southwest Africa. A decline in rainfall is observed over the central Pacific, Ecuador and California, and a slight decrease in rainfall over the Yangtze basin in China and Florida. The Generic Mapping Tools (GMT, <https://github.com/GenericMappingTools/gmt>) was used to create the map.

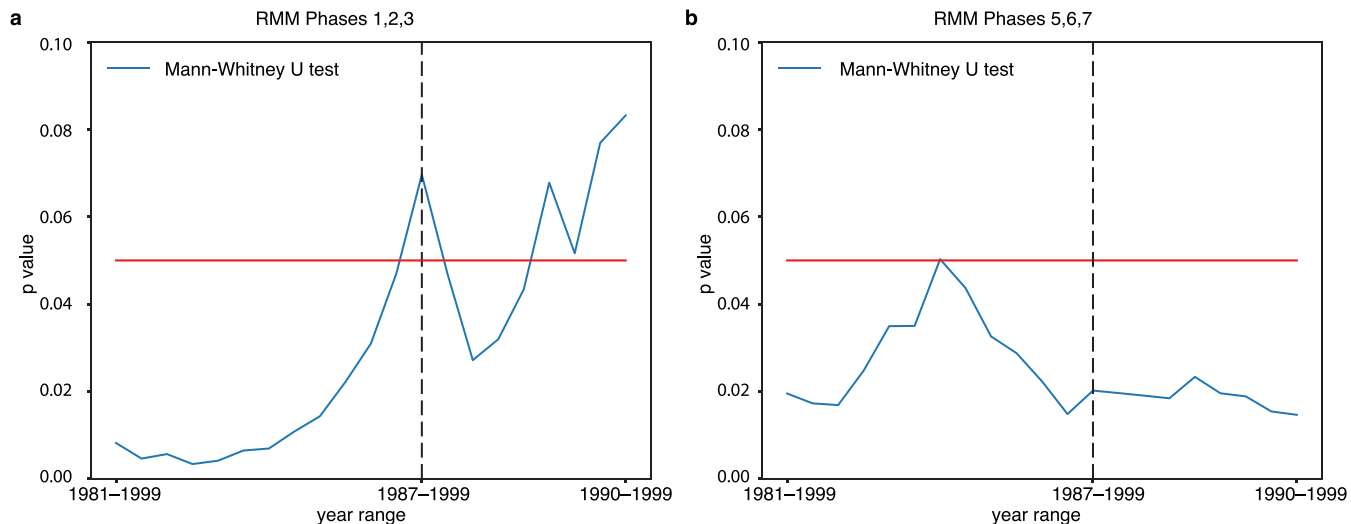
Article

Correlation, Rainfall and MJO phase duration (5, 6, 7)



Extended Data Fig. 7 | Relationship between MJO phase duration and global rainfall, without removing the trends. Correlation between the MJO phase duration (phases 5, 6 and 7) and rainfall anomalies for November–April, during 1981–2018. The correlation analysis is performed after removing the ENSO

variability from the time series, but without removing the trends. Rainfall values are based on the GPCP dataset. The Generic Mapping Tools (GMT, <https://github.com/GenericMappingTools/gmt>) was used to create the map.



Extended Data Fig. 8 | Mann-Whitney *U*-test for testing the significance of the differences in MJO phase duration. The difference in the mean of the MJO phase duration distributions is tested for different starting points. The *P* values are computed for different groups (1981–1999, 1982–1999 to 1990–1999) as the first sample and 2000–2018 as the second sample. **a**, According to the Mann-Whitney *U*-test, the difference in MJO phase duration (1, 2, 3) is statistically

robust ($P < 0.05$, where we can reject the null hypothesis) for the most part of the varying first sample (1981–1999 to 1990–1999, except 1987–1999 where $P = 0.07$). **b**, For the MJO phase duration (5, 6, 7) the difference in mean is always statistically robust (where we can reject the null hypothesis) for the varying first sample (1981–1999 to 1990–1999, where P always < 0.05).